MODELLING MATRIX INJECTION THROUGH ELASTIC POROUS PREFORMS

D. Ambrosi* and L. Preziosi**

* *CRS4: Centro Ricerche e Sviluppo Studi Superiori Sardegna*
Via Nazario Sauro 10, Cagliari, 09123, Italy

** *Dipartimento di Matematica, Politecnico*
Corso Duca degli Abruzzi 24, Torino, 10129, Italy

Abstract. The paper deduces a new model to simulate, under isothermal conditions, some manufacturing processes used to fabricate composites, such as squeeze casting, RTM, and SRIM, in which a melt material is forced into a solid preform. The target of the model is to describe those situations in which infiltration generates deformations in the reinforcing network, both in that part of the solid preform which is still dry and in that part that has been already infiltrated, and to monitor stress and deformation states in the solid preform. The coupled flow/deformation problem in the fully infiltrated region and in the uninfiltrated region is then formulated with the proper evolution equations for the boundaries delimiting the two domains and with the relative boundary and interface conditions. The stationary configuration is analitically determined for general elastic stress-strain and permeability-volume ratio relations. The unsteady problem is solved numerically, putting in evidence the influence of the deformations on the bulk flow and on the propagation of the advancing front.

Keywords: Deformable porous media, composite materials, infiltration.

1. Introduction

Many composite manufacturing processes, such as resin transfer molding, structural resin injection molding, and squeeze casting, can be schematized as infiltration problems through an initially dry porous material.

In modelling these processes, in the literature, the solid preform is usually assumed to be rigid, though several papers [1–13] show photographs or qualitatively describe deformation of the solid preform (see also [14] for a recent review of the subject).

In fact, in several practical situations the preform is far from being rigid and the pressure gradient driving the flow can generate significant deformation, especially ahead the advancing infiltration front and

where the liquid matrix penetrates the preform. Of course, the compression of the preform decreases its permeability hampering the flow.

As will be shown, the evolution of this system, and, in particular, the stationary configuration are very different from that experimentally observed when the coupling between fluid flow and deformation of the porous medium is absent [15]. For this reason deformations need to be taken into account in simulating composite materials manufacturing. Furthermore, from an industrial point of view, it is important to monitor deformation and stress states in the solid preform to identify in advance possible inhomogeneities and damages in the reinforcing network.

Of course, higher infiltration pressures cause stronger deformation and, viceversa, deformations could be, in principle, controlled reducing the applied pressure. There are, however, several reasons for which a sufficiently high pressure need be applied:

i) The mold has to be completely filled before the resin gel cures, or the metal melt solidifies.

ii) The entry of metal melts is usually opposed by the necessity of generating meniscus curvature at the infiltration front. It is therefore, necessary to overcome this adverse capillary pressure before infiltration can even start.

iii) A higher applied pressure reduces the infiltration time, which, in turn, reduces the occurrence of undesired interfacial reactions and degradation of the fibrous reinforcement.

iv) From the industrial point of view it is always desirable to obtain the final product in the shortest time possible, but still in good shape.

In order to determine a satisfactory compromise among the different aspects, one has then to model the whole infiltration process, in order to identify the optimum set of operating parameters and predict a window of applicability in the parameter space as qualitatively attempted in [1, 16, 17].

To this aim this paper will model and simulate the isothermal infiltration process in deformable porous preforms. The problem presents the formation of three time-dependent domains, the first one occupied by the liquid only, the second one by the solid preform wet by the liquid matrix, and the third one consisting of the uninfiltrated solid preform.

It is assumed that a sharp front divides the three domains. If this might be plain for the interface dividing the pure liquid and the wet preform, i.e. one of the borders of the preform, it implies a simplification of capillary phenomena at the interface between the saturated and the dry porous medium. This assumption, often called slug-flow approximation, is reasonable when the applied pressure is much larger than the capillary pressure.

Another non-trivial problem which will be dealt with is the deduction of the evolution equations for the interfaces delimiting the different domains and the formulation of the relative boundary and interface conditions that need be joined to the deformable porous media model.

The stationary problem is analitically determined for general nonlinear elastic stress-strain and permeability-volume ratio relations. A relation between maximum deformation of the preform and the work

parameters (namely, preform dimension, stiffness, and permeability, melt viscosity, and infiltration velocity) is given.

Finally, the unsteady coupled flow/deformation problem, which, under elasticity assumptions, has a hyperbolic structure, is solved by finite differences methods using upwind methods based on characteristic decomposition.

More in details the paper develops as follows. After this introduction, Section 2 presents the isothermal model based on the theory of deformable porous media suitable to simulate squeeze casting, or injection molding processes, in which deformation of the solid preform cannot be neglected and need be monitored. In Section 3 the evolution equations of the interfaces delimiting the time-varying domains and the relative interface and boundary conditions are determined. In Section 4 the steady problem is analytically solved. Finally, Section 5 deals with the numerical method and discusses the results of the simulation of the infiltration process in an initially dry and elastic porous preform under several work conditions.

2. Modelling the Infiltration Process

Squeeze casting and injection molding manufacturing processes can be schematized as infiltration problems of incompressible liquids in deformable porous media made up of an incompressible solid constituent.

The coupled flow/deformation problem can then be described in the framework of the theory of mixtures, which in the isothermal case and in absence of chemical reactions and phase changes can be written as

$$\frac{\partial \phi_s}{\partial t} + \nabla \cdot (\phi_s \mathbf{v}_s) = 0 \tag{2.1}$$

$$\frac{\partial \phi_\ell}{\partial t} + \nabla \cdot (\phi_\ell \mathbf{v}_\ell) = 0 \tag{2.2}$$

$$\rho_s \phi_s \left(\frac{\partial \mathbf{v}_s}{\partial t} + \mathbf{v}_s \cdot \nabla \mathbf{v}_s \right) = \nabla \cdot \tilde{\mathbb{T}}_s + \rho_s \phi_s \mathbf{g} + \mathbf{m} \tag{2.3}$$

$$\rho_\ell \phi_\ell \left(\frac{\partial \mathbf{v}_\ell}{\partial t} + \mathbf{v}_\ell \cdot \nabla \mathbf{v}_\ell \right) = \nabla \cdot \tilde{\mathbb{T}}_\ell + \rho_\ell \phi_\ell \mathbf{g} - \mathbf{m} \tag{2.4}$$

where ρ_s is the density of the solid material used to make the preform, and ρ_ℓ is the density of the liquid matrix to be injected, ϕ_s and ϕ_ℓ are, respectively, the volume fraction of the solid preform and the liquid matrix, i.e. the volume occupied by the constituent over the total volume ($\phi_s + \phi_\ell = 1$), $\mathbf{v}_s$ and $\mathbf{v}_\ell$ are, respectively, the velocity of the solid preform and the liquid matrix, $\tilde{\mathbb{T}}_s$ and $\tilde{\mathbb{T}}_\ell$ are the so-called partial stress tensors, and $\mathbf{m}$ is the so-called interaction force, which describes the microscopic interactions between the solid preform and the liquid matrix across the interface separating them.

The main difficulty in using this theory is in formulating and validating the constitutive relations for the partial stresses, and the interfacial force appearing in it. In particular, neither the partial stresses nor the interfacial force can be tested directly. Information can only be obtained on the basis of thermodynamic arguments classically used in continuum mechanics (see, for instance [18].)

Under some assumptions, however, it is possible to deduce Darcy's law for the infiltration of liquids in deformable porous media from the momentum equation of the liquid constituent

$$\mathbf{v}_\ell - \mathbf{v}_s = -\frac{\mathbb{K}(\mathbb{E}_s)}{\mu \phi_\ell} (\nabla P_\ell - \rho_\ell \mathbf{g}) \ , \tag{2.5}$$

where $\mathbb{K}$ is the permeability tensor, $\mathbb{E}_s$ is the Lagrangian strain tensor, μ is the matrix viscosity, and P_ℓ is the pore liquid pressure (see, for instance, [19], or [14] which focuses on the application to composite materials manufacturing.)

Manipulating the model as done in [20] one can then write

$$\frac{\partial \phi_s}{\partial t} + \nabla \cdot (\phi_s \mathbf{v}_s) = 0 \tag{2.6}$$

$$\nabla \cdot \mathbf{v}_s = \frac{1}{\mu} \nabla \cdot [\mathbb{K}(\mathbb{E}_s)(\nabla P_\ell - \rho_\ell \mathbf{g})] \tag{2.7}$$

$$\rho_s \phi_s \left(\frac{\partial \mathbf{v}_s}{\partial t} + \mathbf{v}_s \cdot \nabla \mathbf{v}_s \right) = \nabla \cdot \mathbb{T}_m + [\rho_s \phi_s + \rho_\ell (1 - \phi_s)]\mathbf{g} \tag{2.8}$$

In this model the only quantity which is still constitutively to be specified is the the stress tensor for the mixture as a whole $\mathbb{T}_m$. Information on it, however, can be obtained using classical continuum mechanics tools and validation can, in principle, be performed, directly by conceiving suitable but standard experiments, aimed at evaluating the dynamical response of the wet solid preform compressed at different volume ratios to oscillatory twist and compression, and to creep and stress relaxation tests.

Unfortunately, the literature lacks of experimental results in this direction. Only Kim, McCarthy and Fanucci [4] performed experiments addressed to the study of the stress relaxation properties of a wet preform finding a spectrum of relaxation times, and several other authors [2, 10, 11, 16] have noticed a viscoelastic behaviour of the materials they use with non-negligible relaxation times.

On the basis of these (mostly qualitative) observations, in [20] it is suggested that the wet preform be modelled as an anelastic solid or as a Voigt-Kelvin solid and experiments in this direction are encouraged. However, at present it is hard to identify the values of the physical parameters involved. In this situation, here it is assumed that both the wet and the dry preform respond elastically to deformations.

Furthermore, it is assumed that the solid preform undergoes one-dimensional infiltration and deformation along a principal direction of the preform permeability tensor.

The dry preform occupies for $t < 0$ the region $x \in [0, L]$ and is compressed at a given volume ratio $\phi_s(x, t = 0) = \phi_0(x)$, or possibly it is in its undeformed configuration $\phi_s(x, t = 0) = \phi_r$.

The right border of the solid preform is constrained by a net which prevents the preform from being pushed beyond $x = L$, but allows, at the same time, both air and liquid matrix to pass through with no resistance (see Fig. 1).

The liquid matrix flows in the positive direction either pushed at a given velocity, or forced by a pressure gradient. At $t = 0$, it touches the free border $x = 0$ of the solid preform.

The incoming liquid compresses the sponge and starts infiltrating. Therefore, while the right border of the sponge is fixed at $x = L$, the other one moves to $x = x_f(t)$, and part of the preform wets, say up to $x = x_i(t)$.

In doing this we are implicitly simplifying capillary phenomena assuming the existence of a sharp flat front, which divides the fully saturated porous medium $\mathcal{D}^w = [x_f(t), x_i(t)]$ from the remaining uninfiltrated portion $\mathcal{D}^d = [x_i(t), L]$. This assumption, often called slug-flow approximation, is valid when the applied pressure is much larger than the capillary pressure.

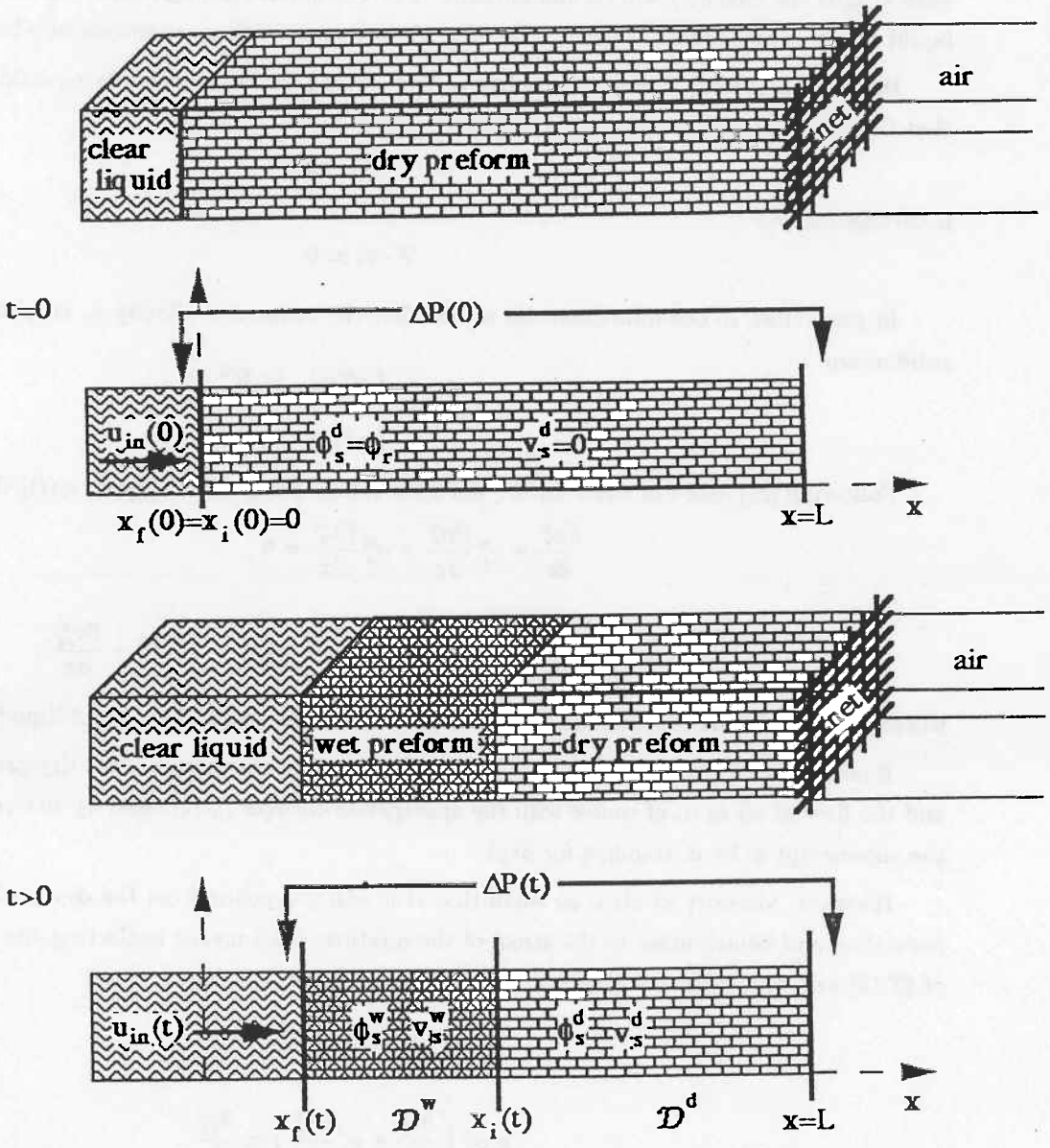

Figure 1 — Geometrical schematization of the infiltration problem.

As infiltration proceeds both the dry and the wet preform compress or expand back, according to the flow conditions. However, as will be shown in Section 4, even long after the liquid matrix has reached the other end of the sponge $x = L$, the final steady configuration (which can be reached if the liquid is steadily pushed into the channel) will be non-uniform. The undeformed configuration can be reached again only if liquid inflow is stopped and further relaxation of the sponge with spontaneous imbibition is allowed.

Before proceeding, it is useful to observe that adding the two continuity equations (2.1)–(2.2) one has that the so-called composite velocity

$$\mathbf{v}_c = \phi_s \mathbf{v}_s + \phi_\ell \mathbf{v}_\ell \,, \tag{2.9}$$

is divergence-free

$$\nabla \cdot \mathbf{v}_c = 0 \,. \tag{2.10}$$

In particular, in one dimension this means that the composite velocity v_c is space independent in each subdomain

$$v_c(x,t) = \begin{cases} v_c^w(t) & \text{in } \mathcal{D}^w \,; \\ v_c^d(t) & \text{in } \mathcal{D}^d \,. \end{cases} \tag{2.11}$$

Following [20], one can write for the wet part of the sponge $\mathcal{D}^w = [x_f(t), x_i(t)]$ the following model

$$\frac{\partial \phi_s^w}{\partial t} + v_s^w \frac{\partial \phi_s^w}{\partial x} + \phi_s^w \frac{\partial v_s^w}{\partial x} = 0 \,, \tag{2.12}$$

$$\rho_s \phi_s^w \left(\frac{\partial v_s^w}{\partial t} + v_s^w \frac{\partial v_s^w}{\partial x} \right) = -\frac{\mu}{K(\phi_s^w)} [v_s^w - v_c^w(t)] + \frac{\partial \tau_m^w}{\partial x} \,, \tag{2.13}$$

where the superscript w stands for *wet*, and τ_m^w is the excess stress of the solid-liquid mixture.

Equations (2.12)–(2.13) could also be applied to describe the motion of the dry preform in $\mathcal{D}^d = [x_i(t), L]$ and the flow of air in it, of course with the appropriate changes (μ replaced by the viscosity of air μ_{air}, and the superscript w by d, standing for *dry*).

However, viscosity of air is so small that it is easily expelled from the dry preform offering negligible resistance and contribution to the stress of the mixture. This means neglecting the first term on the r.h.s. of (2.13) and approximate τ_m^d with τ_s^d. One can then write

$$\frac{\partial \phi_s^d}{\partial t} + v_s^d \frac{\partial \phi_s^d}{\partial x} + \phi_s^d \frac{\partial v_s^d}{\partial x} = 0 \,, \tag{2.14}$$

$$\rho_s \phi_s^d \left(\frac{\partial v_s^d}{\partial t} + v_s^d \frac{\partial v_s^d}{\partial x} \right) = \frac{\partial \tau_s^d}{\partial x} \,. \tag{2.15}$$

Equation (2.15) can be also obtained considering Eq.(2.3) and assuming that the gas is easily expelled from the dry preform generating negligible interfacial interaction and influence on the partial stress of the solid constituent.

As already stated, due to the scarsity of experimental data on the viscoelastic properties of both the wet and dry preform, in this paper it will be assumed that they behave elastically

$$\tau_m^w = -\Sigma_m(\phi_s^d) \,, \qquad \text{in} \quad \mathcal{D}^w \,, \tag{2.16}$$

$$\tau_s^d = -\Sigma_s(\phi_s^d) \,, \qquad \text{in} \quad \mathcal{D}^d \,, \tag{2.17}$$

with Σ_m and Σ_s strictly increasing functions of the volume ratio. Under this assumption the system of equations (2.12)–(2.15) is hyperbolic.

We finally observe that most papers in the literature measure $\Sigma_s(\phi_s)$ and assume, more or less implicitly, that

$$\Sigma_s(\phi_s) = \Sigma_m(\phi_s) \ , \tag{2.18}$$

which means assuming that the response of the porous material is independent on its being dry or wet.

This step can be considered an approximation, since from a continuum mechanics viewpoint, Σ_m contains other contributions besides Σ_s, such as the stress in the liquid and a fluctuation term [14]. Besides, from an experimental viewpoint, several authors have shown that the static response of a porous medium depends on whether it is dry or wet. For instance, Beavers and coworkers [21–23] explicitly observe "a reduction in the compressive force when a specimen is completely saturated and submerged in water for all polyurethane foams (...) used in the experiments. Although the mechanism underlying this behavior cannot be identified with certainty, it is believed that the liquid (i.e., water) tends to lubricate the deforming solid and therefore diminishes the resistance to deformation." This is also a matter of common experience, when squeezing some sponges before and after dipping them into a liquid.

3. Interface and Boundary Conditions

In order to close the system, we have still to add proper interface and boundary conditions to (2.12)–(2.15) and give the evolution equations for the interface $x_i(t)$ and the free boundary $x_f(t)$.

The sponge borders $x = x_f(t)$ and $x = L$ are material interfaces fixed on the solid phase, while $x = x_i(t)$ is a material interface fixed on the liquid phase.

Following Liu [24] and Müller [25], one can deduce for (2.6)–(2.8) the following set of interface conditions

$$[\![\mathbf{v}_c]\!] \cdot \mathbf{n} = 0 \ , \tag{3.1}$$

$$[\![\mathbb{T}_m \mathbf{n} - \rho_s \phi_s \mathbf{v}_s (\mathbf{v}_s - \mathbf{v}_\sigma) \cdot \mathbf{n}]\!] = 0 \ , \tag{3.2}$$

where $[\![\mathbf{f}]\!]$ denotes the jump of $\mathbf{f}$ across the interface σ dividing the domains, $\mathbf{n}$ the normal to the interface, and $\mathbf{v}_\sigma$ is the velocity of the interface. These conditions represent continuity of the fluxes through the interface, that is conservation of mass and momentum.

According to (3.1), the composite velocity is continuous across each material interface and according to (2.11) is constant in each domain. Therefore, going all the way down where there is only pure liquid, one has that the composite velocity is everywhere equal to the inflow velocity

$$v_c(x,t) = v_c^w(t) = v_c^d(t) = u_{in}(t) \qquad \forall x \in \mathcal{D}^w \cup \mathcal{D}^d \ . \tag{3.3}$$

In particular, in $\mathcal{D}^w$

$$v_\ell^w(x,t) = \frac{u_{in}(t) - \phi_s^w(x,t) v_s^w(x,t)}{1 - \phi_s^w(x,t)} \ . \tag{3.4}$$

Since $x = x_i(t)$ is a material interface fixed on the liquid phase it has to move with the velocity of the liquid at the interface. Therefore,

$$\frac{dx_i}{dt} = \frac{u_{in}(t) - \phi_s^w(x_i(t),t)v_s^w(x_i(t),t)}{1 - \phi_s^w(x_i(t),t)} \ . \tag{3.5}$$

On the other hand, $x_f(t)$ is a material interface fixed on the solid phase and, therefore, it has to move with the velocity of the solid at the interface

$$\frac{dx_f}{dt} = v_s^w(x_f(t),t) \ . \tag{3.6}$$

This also reduces Eq.(3.2) to a stress continuity condition across $x_f(t)$. Since the liquid pressure is continuous across the interface, too, then Eq.(3.2) simplifies to

$$\tau_m^w(x_f(t),t) = -\Sigma_m(\phi_s^w(x_f(t),t)) = 0 \ , \tag{3.7}$$

that is the free border of the preform is locally in the undeformed state

$$\phi_s^w(x_f(t),t) = \phi_r^w \tag{3.8}$$

implicitly defined by (3.7).

Of course, since the other border $x = L$ of the solid preform is constrained by a net

$$v_s^d(L,t) = 0 \ . \tag{3.9}$$

At the interface $x_i(t)$, where $v_\sigma = \frac{dx_i}{dt} = v_\ell^w$, Eq.(3.1) specializes to

$$\phi_s^d v_s^d - \phi_s^u v_s^w = (\phi_s^d - \phi_s^w)v_\ell^w \ , \tag{3.10}$$

where v_ℓ^w is given by (3.4), and all variables are computed in $(x_i(t),t)$.

The stress condition, instead, writes

$$\Sigma_s(\phi_s^d) + \rho_s\phi_s^d v_s^d(v_s^d - v_\ell^u) = \Sigma_m(\phi_s^w) + \rho_s\phi_s^w v_s^w(v_s^w - v_\ell^w) \ . \tag{3.11}$$

The interface conditions (3.10)–(3.11) are not in closed form as (3.8) and (3.9), because they couple the solution between the domains. They correctly obey to the characteristics theory, as the systems of equations (2.12)–(2.13) and (2.14)–(2.15) require one boundary condition each.

Substituting (3.4) evaluated in $x_i(t)$ and carrying out some calculations, one can put in evidence the following relations

$$v_s^w = \frac{(\phi_s^w - \phi_s^d)u_{in}(t) + (1 - \phi_s^w)\phi_s^d v_s^d}{(1 - \phi_s^d)\phi_s^w} \ , \tag{3.12a}$$

$$\Sigma_s(\phi_s^w) - \Sigma_m(\phi_s^d) = \rho_s \frac{\phi_s^d(\phi_s^w - \phi_s^d)[v_s^d - u_{in}(t)]^2}{(1 - \phi_s^d)^2\phi_s^w} \ . \tag{3.12b}$$

It is to be mentioned that the dependence of Σ on ϕ, which must be deduced from experimental measurements, must in general be such that the relationships (3.12) are single-valued. If, for instance, it is assumed that the wet and dry porous material behave elastically and in the same way (i.e., Eq.(2.18) holds), one has that

$$v_s^w(x_i(t),t) = v_s^d(x_i(t),t) \ , \tag{3.13a}$$

$$\phi_s^w(x_i(t),t) = \phi_s^d(x_i(t),t) \ , \tag{3.13b}$$

which means that both the volume ratio and the velocity of the solid constituent are continuos across $x_i(t)$.

As already mentioned, however, at the end of Section 2 this is not genuinely true, since different constitutive models should be used in the two domains. Using the same constitutive equation and stress-strain relation in the two domains, and therefore (3.13), is to be considered an approximation.

The initial boundary value problem is then given by Eqs.(2.12)–(2.15) joined with the evolution equation for the interfaces (3.5)–(3.6), the boundary and interface conditions (3.8)–(3.11) (we remind that the quantities appearing in (3.9) and (3.10) are evaluated at $(x_i(t),t)$), and the initial conditions

$$\begin{cases} \phi_s^d(x,0) = \phi_r & \text{for } 0 \le x \le L, \\ v_s^d(x,0) = 0 & \text{for } 0 \le x \le L, \\ x_f(0) = 0 \ , \\ x_i(0) = 0 \ , \end{cases} \tag{3.14}$$

if $x_i(t) < L$, that is for $t < \frac{(1-\phi_r)L}{u_{in}}$ if u_{in} is constant.

When the solid preform is fully infiltrated, i.e. $\mathcal{D}^d = \emptyset$, then the integration of the initial boundary value problem continues with Eqs.(2.12)–(2.13) with the evolution equation (3.6), and the boundary conditions (3.8) and

$$v_s^w(L,t) = 0 \ . \tag{3.15}$$

The quantity $u_{in}(t)$ which appears in the initial boundary value problem depends on how the liquid matrix is injected in the solid preform. If the liquid is pushed by a piston at a given velocity, then $u_{in}(t)$ is actually a given function of time, e.g. $u_{in} = \text{const}$.

A more interesting situation arises when the flow is driven by a prescribed pressure difference

$$\Delta P_\ell(t) = P_\ell(x_f(t),t) - P_\ell(L,t) \ , \tag{3.16}$$

applied between the extrema of the solid preform (say, constant).

From (2.5), (2.9), and (3.3) written in one dimension, one can explicitly write the velocity of the constituents as

$$v_s^w = u_{in}(t) + \frac{K(\phi_s^w)}{\mu}\frac{\partial P_\ell}{\partial x} \ , \tag{3.17}$$

$$v_s^d = u_{in}(t) + \frac{K(\phi_s^d)}{\mu_{air}}\frac{\partial P_\ell}{\partial x} \ , \tag{3.18}$$

or

$$\frac{\partial P_\ell}{\partial x}(x,t) = \begin{cases} \dfrac{\mu}{K(\phi_s^w(x,t))}[v_s^w(x,t) - u_{in}(t)] & \text{in } \mathcal{D}^w; \\ \dfrac{\mu_{air}}{K(\phi_s^d(x,t))}[v_s^d(x,t) - u_{in}(t)] & \text{in } \mathcal{D}^d. \end{cases} \tag{3.19}$$

Integrating (3.19) over $[x_f(t), L]$ gives

$$\begin{aligned} \Delta P_\ell(t) = &- \mu \int_{x_f(t)}^{x_i(t)} \frac{v_s^w(x,t)\,dx}{K(\phi_s^w(t,x))} - \mu_{air} \int_{x_i(t)}^{L} \frac{v_s^d(x,t)\,dx}{K(\phi_s^d(t,x))} \\ &+ u_{in}(t) \left[\mu \int_{x_f(t)}^{x_i(t)} \frac{dx}{K(\phi_s^w(t,x))} + \mu_{air} \int_{x_i(t)}^{L} \frac{dx}{K(\phi_s^d(t,x))} \right]. \end{aligned} \tag{3.20}$$

which can be explicited with respect to u_{in} as

$$u_{in}(t) = \frac{\dfrac{\Delta P_\ell(t)}{\mu} + \displaystyle\int_{x_f(t)}^{x_i(t)} \frac{v_s^w(x,t)\,dx}{K(\phi_s^w(t,x))} + \frac{\mu_{air}}{\mu} \int_{x_i(t)}^{L} \frac{v_s^d(x,t)\,dx}{K(\phi_s^d(t,x))}}{\displaystyle\int_{x_f(t)}^{x_i(t)} \frac{dx}{K(\phi_s^w(t,x))} + \frac{\mu_{air}}{\mu} \int_{x_i(t)}^{L} \frac{dx}{K(\phi_s^d(t,x))}}. \tag{3.21}$$

Since the viscosity of the gas is much smaller than the viscosity of the infiltrating liquid, then the pressure drop in $\mathcal{D}^d$ is negligible, which reduces Eq.(3.21) to

$$u_{in}(t) = \frac{\dfrac{\Delta P_\ell(t)}{\mu} + \displaystyle\int_{x_f(t)}^{x_i(t)} \frac{v_s^w(x,t)\,dx}{K(\phi_s^w(t,x))}}{\displaystyle\int_{x_f(t)}^{x_i(t)} \frac{dx}{K(\phi_s^w(t,x))}}. \tag{3.22}$$

However, in our problem initially $x_i(0) = x_f(0) = 0$ and therefore at the very beginning $x_i(t)$ and $x_f(t)$ are very close. At this early stages of infiltration one should then consider the full relation (3.21), instead of (3.22). In fact, for

$$\frac{x_i(t) - x_f(t)}{L} \approx \frac{\mu_{air}}{\mu},$$

the two integrals at the denominator may be of the same order of magnitude.

Using standard work parameters this occurs at most for $t < 0.001 - 0.01\ sec$ yielding an initial inflow velocity of the order of one meter per second.

4. Steady State and Analytic Solution

Assume that the input velocity $u_{in}(t)$ of the liquid, or, equivalently, the pressure gradient driving the flow, tends to a constant. In this situation one may look for stationary solution in which the solid preform is all wet and at rest at a volume ratio $\phi_s^w(x,t) = \phi_s^\infty(x)$. In order to describe this state, we will drop, for sake of clarity, the superscript ∞, observing that in this section all variables are time independent.

From Eq.(2.13) we can then write

$$\frac{\mu u_{in}}{K(\phi_s)} = \Sigma'(\phi_s)\frac{\partial \phi_s}{\partial x} \qquad \text{for} \qquad x \in [x_f, L] \,, \tag{4.1}$$

where

$$\Sigma'(\phi_s) = \frac{d\Sigma}{d\phi_s} > 0 \,, \tag{4.2}$$

and Eq.(3.8) can be rewritten as

$$\phi_s(x_f) = \phi_r \,. \tag{4.3}$$

Equation (4.3) does not provide a proper initial condition to solve the ordinary differential equation (4.1), since it gives the volume ratio ($\phi_s = \phi_r$) in a location $x = x_f$ to be determined. On the other hand, the volume ratio at the fixed end of the solid preform and the length of the compressed preform are unknown. As we shall see, the mass of the solid preform, which is constant throughout the evolution of the system, will furnish the necessary information to solve the problem.

Integrating (4.1) gives

$$\mu u_{in}(x - L) = \int_{\phi_s(L)}^{\phi_s(x)} K(\psi)\Sigma'(\psi)\, d\psi \,, \tag{4.4}$$

where, as already mentioned, $\phi_s(L)$ is still to be deteremined.

Given a volume ratio $\phi_s \in [\phi_r, \phi_s(L)]$, Eq.(4.4) gives the locations where it is assumed

$$x(\phi_s) = L - \frac{1}{\mu u_{in}} \int_{\phi_s}^{\phi_s(L)} K(\psi)\Sigma'(\psi)\, d\psi \,. \tag{4.5}$$

In particular,

$$x_f = L - \frac{1}{\mu u_{in}} \int_{\phi_r}^{\phi_s(L)} K(\psi)\Sigma'(\psi)\, d\psi \,. \tag{4.6}$$

The value $\phi_s(L)$ which appears in (4.4)–(4.6) can be obtained recalling that the mass of the sponge is preserved during the evolution. In particular, it is equal to the mass at time $t = 0$

$$\phi_r L = \int_{x_f}^{L} \phi_s(x)\, dx \,. \tag{4.7}$$

If $\Sigma(\phi_s)$ is strictly increasing, then from (4.1) also $\phi_s(x)$ is strictly increasing. Transforming the integral over x in an integral over ϕ_s gives

$$\int_{x_f}^{L} \phi_s(x)\, dx + \int_{\phi_r}^{\phi_s(L)} x(\phi_s)\, d\phi_s + \phi_r x_f = \phi_s(L) L \,. \tag{4.8}$$

or, using (4.7) and then (4.5).

$$\begin{aligned} \phi_r L =& \phi_s(L) L - \phi_r x_f - \int_{\phi_r}^{\phi_s(L)} x(\phi_s)\, d\phi_s \\ =& \phi_r(L - x_f) + \frac{1}{\mu u_{in}} \int_{\phi_r}^{\phi_s(L)} \int_{\phi}^{\phi_s(L)} K(\psi)\Sigma'(\psi)\, d\psi \cdot d\phi \,. \end{aligned} \tag{4.9}$$

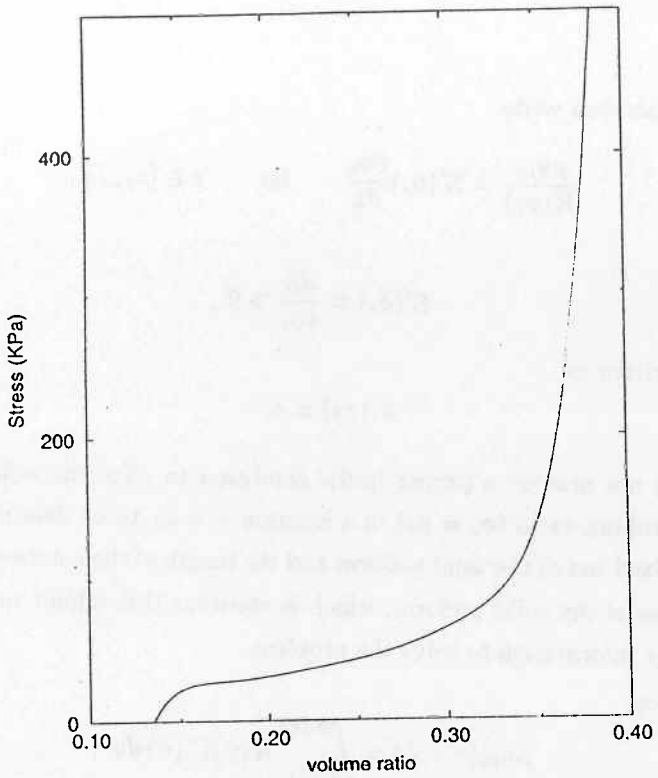

Figure 2 — Stress-volume ratio relation as measured by Sommer and Mortensen [10] for a polyurethane sponge.

Changing order of integration in the double integral one can write

$$\begin{aligned}\phi_r x_f &= \frac{1}{\mu u_{in}} \int_{\phi_r}^{\phi_s(L)} K(\psi)\Sigma'(\psi) \left(\int_{\phi_r}^{\psi} d\phi_s \right) d\psi \\ &= \frac{1}{\mu u_{in}} \int_{\phi_r}^{\phi_s(L)} K(\psi)\Sigma'(\psi)(\psi - \phi_r)\, d\psi \\ &= \frac{1}{\mu u_{in}} \int_{\phi_r}^{\phi_s(L)} K(\phi_s)\Sigma'(\phi_s)\phi_s\, d\phi_s - \frac{\phi_r}{\mu u_{in}} \int_{\phi_r}^{\phi_s(L)} K(\phi_s)\Sigma'(\phi_s)\, d\phi_s \,.\end{aligned} \tag{4.10}$$

Using (4.6), Eq.(4.10) can be simplified into

$$\mu u_{in} \phi_r L = \int_{\phi_r}^{\phi_s(L)} K(\phi_s)\Sigma'(\phi_s)\phi_s\, d\phi_s \,, \tag{4.11}$$

which is an integral relation implicitly defining $\phi_s(L)$.

Once $K(\phi_s)$ and $\Sigma(\phi_s)$ are given, and $\phi_s(L)$ is computed using (4.11), the steady solution is given by (4.5) and, in particular, the location of the free border by (4.6).

It has to be observed that, since the integrands are all positive, $\phi_s(L)$ and x_f are increasing functions of u_{in}. This means that, unless $u_{in} = 0$, or, equivalently, $\Delta P_t = 0$, $x_f > 0$ and the preform is neither relaxed nor uniformly compressed. As expected, however, if the viscosity or the inflow velocity are very small, or if the solid preform is very stiff, then the steady configuration of the preform is nearly undeformed.

As an example we will now consider the permeability-volume ratio relation and the stress-volume ratio relation measured by Sommer and Mortensen [10] for a polyurethane sponge (TF-5070-10), namely

$$K(\phi_s) = 1.4729 \cdot 10^{-10-6.9654\phi_s} \text{ m}^2$$
$$\Sigma(\phi_s) = \left(\sum_{k=0}^{7} a_k \phi_s^k \right) \text{ MPa} \tag{4.12}$$

with

$$a_0 = -23.29164\,, \quad a_1 = 713.49318\,, \quad a_2 = -9255.285\,, \quad a_3 = 65974.87\,,$$
$$a_4 = -279182.3\,, \quad a_5 = 701653.83\,, \quad a_6 = -970226.7\,, \quad a_7 = 569801.8\,,$$

(see Figure 2), which, in particular, yield the following values in the undeformed configuration

$$\phi_r = 0.135175\,, \quad \Sigma'(\phi_r) = 2.522532 \text{ MPa} \quad \text{and} \quad K(\phi_r) = 1.6851 \cdot 10^{-11} \text{ m}^2\,.$$

Figure 3 gives the stationary configuration $\phi_s(x/L)$ at different values of the dimensionless parameter

$$\mathcal{S} = \frac{\Sigma'(\phi_r) K(\phi_r)}{\mu u_{in} L}\,. \tag{4.13}$$

Therefore, higher values of $\mathcal{S}$ correspond, for instance, to stiffer, or more permeable solid preforms, less viscous fluids, smaller inflow velocities.

Clearly, the smaller $\mathcal{S}$ is, the more inhomogeneous the steady configuration is.

In Figure 4 the ratio of the position of the preform border over its undeformed length, i.e. x_f/L, and the value of the volume ratio at the fixed end of the sponge $x = L$ (which, in the stationary configuration, is the maximum preform deformation) are plotted versus $\mathcal{S}$. Again the higher $\mathcal{S}$ is, the less deformed the solid preform is. In particular, Fig. 4 and the original Eq.(4.6) and (4.11) give an indication of the work parameters that can be possibly used to control preform deformation.

The case in which the pressure gradient ΔP_ℓ is imposed and eventually constant is somewhat different, but easier. In fact, from the stress equilibrium equation, one directly has

$$\phi_s(x = L) = \Sigma^{-1}(\Delta P_\ell)\,, \tag{4.14}$$

which can be used as "initial" condition to solve the ordinary differential equation. However, the constant u_{in} in (4.1) is not given explicitly, but depends on the dimension and the deformation of the solid preform. However, as before, the fact that the total mass is given determines

$$u_{in} = \frac{1}{\mu \phi_r L} \int_{\phi_r}^{\Sigma^{-1}(\Delta P_\ell)} K(\phi_s)\Sigma'(\phi_s)\phi_s \, d\phi_s\,, \tag{4.15}$$

which can be substituted in (4.5) and (4.6) to have

$$x(\phi_s) = L \left(1 - \phi_r \frac{\displaystyle\int_{\phi_s}^{\Sigma^{-1}(\Delta P_\ell)} K(\psi)\Sigma'(\psi)\, d\psi}{\displaystyle\int_{\phi_r}^{\Sigma^{-1}(\Delta P_\ell)} K(\psi)\Sigma'(\psi)\psi \, d\psi} \right)\,, \tag{4.16}$$

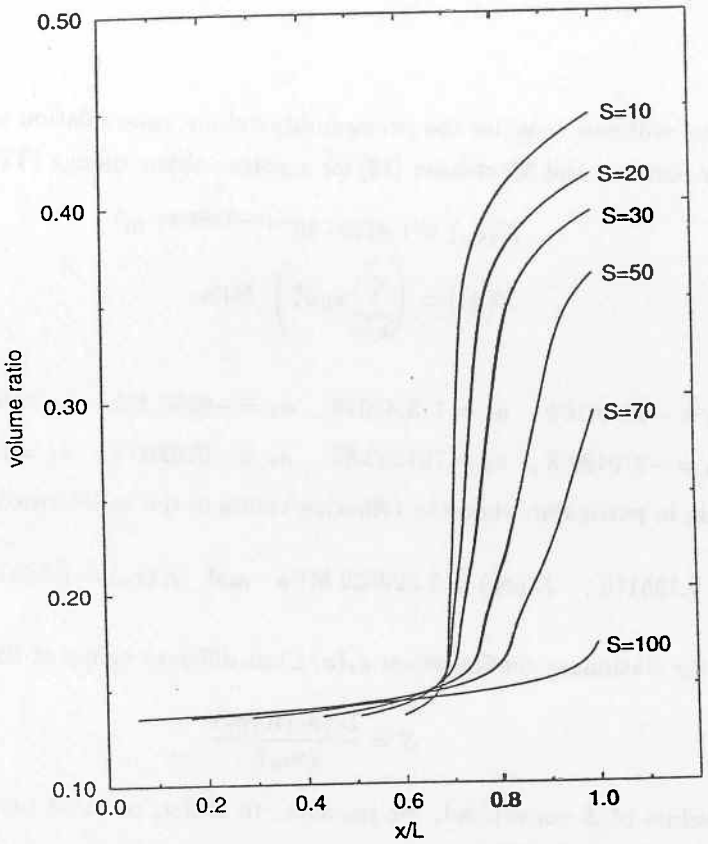

Figure 3 — Stationary state. Volume ratio versus x/L at different values of $\mathcal{S} = \frac{\Sigma'(\phi_r)K(\phi_r)}{\mu u_{in} L}$.

and, in particular,

$$x_f = L\left(1 - \phi_r \frac{\displaystyle\int_{\phi_r}^{\Sigma^{-1}(\Delta P_\ell)} K(\psi)\Sigma'(\psi)\,d\psi}{\displaystyle\int_{\phi_r}^{\Sigma^{-1}(\Delta P_\ell)} K(\psi)\Sigma'(\psi)\psi\,d\psi}\right). \tag{4.17}$$

5. Simulation Method and Results

As already mentioned in Section 2, the system of equations (2.12)–(2.15) to be integrated is hyperbolic. It turns then useful to write it in conservation form, introducing the fluxes $q_s^w = \phi_s^w v_s^w$, and $q_s^d = \phi_s^d v_s^d$, and the dimensionless variables obtained scaling lengths with the initial length of the preform L, velocities with a characteristic velocity U, and time with L/U.

If $u_{in}(t)$ is specified, then U is its order of magnitude $\widehat{u}_{in}$. If, instead, $\Delta P_\ell(t)$ is specified and $\widehat{P}_\ell$ is its order of magnitude, then $U = \Delta\widehat{P}_\ell K(\phi_r^d)/\mu L$.

The dimensionless system of equations then writes

$$\frac{\partial \phi_s^w}{\partial t} + \frac{\partial q_s^w}{\partial x} = 0\,, \tag{5.1}$$

$$\mathcal{P}\frac{\partial q_s^w}{\partial t} + \frac{\partial}{\partial x}\left[\mathcal{P}\frac{(q_s^w)^2}{\phi_s^w} + \mathcal{S}\widetilde{\Sigma}_m(\phi_s^w)\right] = \frac{1}{\widetilde{K}(\phi_s^w)}\left[\widetilde{u}_{in}(t) - \frac{q_s^w}{\phi_s^w}\right]\,, \tag{5.2}$$

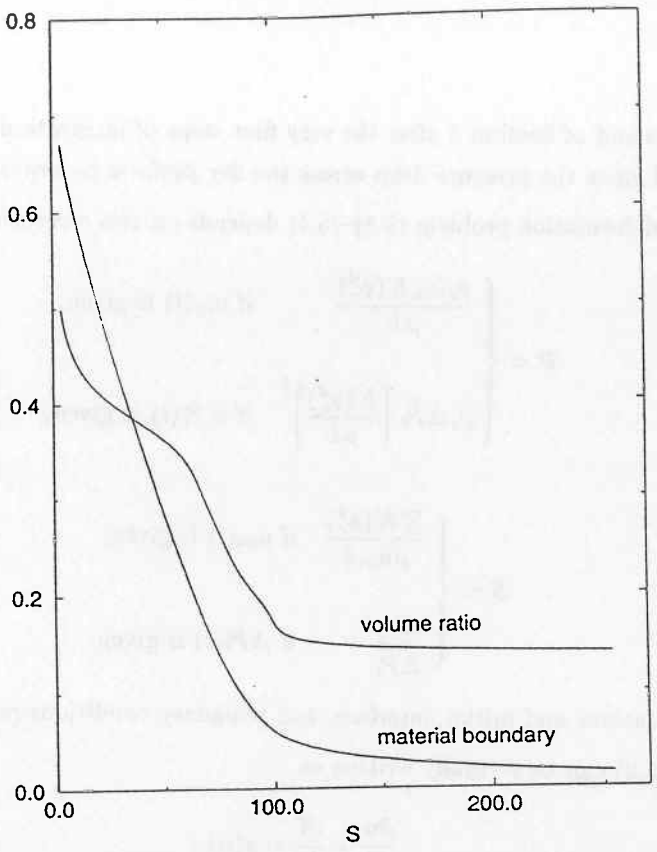

Figure 4 — Stationary state. Dimensionless position of the material boundary x_f/L and volume ratio $\phi_s(L)$ at the fixed boundary as a function of $\mathcal{S} = \frac{\Sigma'(\phi_r)K(\phi_r)}{\mu u_{in} L}$.

$$\frac{\partial \phi_s^d}{\partial t} + \frac{\partial q_s^d}{\partial x} = 0 \,, \tag{5.3}$$

$$\mathcal{P}\frac{\partial q_s^d}{\partial t} + \frac{\partial}{\partial x}\left[\mathcal{P}\frac{(q_s^d)^2}{\phi_s^d} + \mathcal{S}\tilde{\Sigma}_s(\phi_s^d)\right] = 0 \,, \tag{5.4}$$

where now x, t, q_s^d and q_s^w are dimensionless variables,

$$\begin{aligned} \tilde{K}(\phi_s^w) &= \frac{K(\phi_s^w)}{K(\phi_r^d)} \,, \\ \tilde{\Sigma}_m(\phi_s^w) &= \frac{\Sigma_m(\phi_s^w)}{\Sigma'} \,, \\ \tilde{\Sigma}_s(\phi_s^d) &= \frac{\Sigma_s(\phi_s^d)}{\Sigma'} \,, \end{aligned} \tag{5.5}$$

with

$$\Sigma' = \frac{d\Sigma_s}{d\phi_s}(\phi_r^d)$$

and

$$\tilde{u}_{in}(t) = \begin{cases} \dfrac{u_{in}(t)}{\hat{u}_{in}} & \text{if } u_{in}(t) \text{ is given;} \\[2ex] \dfrac{\dfrac{\Delta P_\ell(t)}{\hat{\Delta} P_\ell} + \displaystyle\int_{x_f(t)}^{x_i(t)} \frac{v_s^w(x,t)\,dx}{\tilde{K}(\phi_s^w(t,x))} + \frac{\mu_{air}}{\mu}\int_{x_i(t)}^{1} \frac{v_s^d(x,t)\,dx}{\tilde{K}(\phi_s^d(t,x))}}{\displaystyle\int_{x_f(t)}^{x_i(t)} \frac{dx}{\tilde{K}(\phi_s^w(t,x))} + \frac{\mu_{air}}{\mu}\int_{x_i(t)}^{1} \frac{dx}{\tilde{K}(\phi_s^d(t,x))}} & \text{if } \Delta P_\ell(t) \text{ is given.} \end{cases} \tag{5.6}$$

As explained at the end of Section 3 after the very first steps of integration the integrals over $[x_i(t), L]$ in (5.6) can be dropped since the pressure drop across the dry preform becomes negligible.

The coupled flow/deformation problem (5.1)–(5.4) depends on two dimensionless parameters

$$\mathcal{P} = \begin{cases} \dfrac{\rho_s \widehat{u}_{in} K(\phi_r^d)}{\mu L} & \text{if } u_{in}(t) \text{ is given;} \\ \\ \rho_s \Delta \widehat{P}_\ell \left[\dfrac{K(\phi_r^d)}{\mu L}\right]^2 & \text{if } \Delta P_\ell(t) \text{ is given;} \end{cases} \tag{5.7a}$$

and

$$\mathcal{S} = \begin{cases} \dfrac{\Sigma' K(\phi_r^d)}{\mu \widehat{u}_{in} L} & \text{if } u_{in}(t) \text{ is given;} \\ \\ \dfrac{\Sigma'}{\Delta \widehat{P}_\ell} & \text{if } \Delta P_\ell(t) \text{ is given.} \end{cases} \tag{5.7b}$$

The remaining equations and initial, interface, and boundary conditions remain formally unchanged.

Equations (5.1), (5.2) can be formally written as

$$\frac{\partial \mathbf{u}}{\partial t} + \frac{\partial \mathbf{f}}{\partial x} = \mathbf{s}(\mathbf{u}) \,, \tag{5.8}$$

where

$$\mathbf{u} = (\phi, \mathcal{P}q), \qquad \mathbf{f} = \left(q, \mathcal{P}\frac{q^2}{\phi} + \mathcal{S}\Sigma\right), \qquad \mathbf{s} = \left(0, \frac{u_{in}(t) - \frac{q}{\phi}}{\widetilde{K}(\phi)}\right) . \tag{5.9}$$

Equations (5.3), (5.4) are formally the same, but for the vanishing of the source term $\mathbf{s}$.

For numerical purposes, as the integration domain stretches in time it is useful to consider the integral formulation of the equation above, because at a discrete level it allows to take easily into account of the movements of the grid nodes. The integral formulation of the conservation law (5.8) reads [26]

$$\frac{\partial}{\partial t}\int_{x_1(t)}^{x_2(t)} \mathbf{u} dx + \frac{\partial}{\partial x}\int_{x_1(t)}^{x_2(t)} \mathbf{f} dx = \int_{x_1(t)}^{x_2(t)} \mathbf{s}(\mathbf{u}) \,, \qquad \forall (x_1(t), x_2(t)) \subseteq (x_f(t), x_i(t)) \,. \tag{5.10}$$

where $\mathbf{u}, \mathbf{s}$ have already been defined, and $\mathbf{f}$, defined now as

$$\mathbf{f} = \left(q - v'\phi, \mathcal{P}q\left(\frac{q}{\phi} - v'\right) + \mathcal{S}\Sigma\right) \,, \tag{5.11}$$

takes into account of the movement of the extrema of the interval $(x_1(t), x_2(t))$.

This is the form of the flux vector when considering possibly moving domains with velocity $v'(x,t)$. The contribution of the flux due to v' says that the total quantity of $\mathbf{u}$ in the interval $(x_1(t), x_2(t))$ changes in time as it flows through the boundary of the material because of the movement of the extrema. As the whole solid preform lays in $(x_i(t), L)$ we divide this region into N equally spaced intervals; the discrete solution u_i is defined in the i-th interval, while the $N+1$ numerical fluxes f_i, $i = 0, ...N$, are defined at the border of the intervals. This allows to impose naturally the boundary conditions on the value of the fluxes, as discussed in Section 3.

Referring to the discussion at the end of Section 2, in the simulation we assume that the mechanical properties of the wet and dry solid preform are the same, which imply continuity of volume ratio and velocity at the interface $x_i(t)$ dividing the domains (see(3.13)).

This allows a simplification in handling the interface $x_i(t)$, which can just be treated as a marker, indicating what is the portion of the computational domain that includes a source term in the equations. Conversely, the movement of the material boundary $x_f(t)$ requires a real stretching of the computational domain. This poses some problems, if the movement of the solid is to be taken into account, while preserving a constant distance between the discretizations nodes. This is accomplished by imposing a proper discrete mesh velocity movement $v_i'^n$, $i = 0, ...N$, such that the discretized counterpart of equation (5.10) reads

$$\frac{1}{\Delta t}\left[(\Delta x)^{n+1}\mathbf{u}_i^{n+1} - (\Delta x)^n\mathbf{u}_i^n\right] + (\Delta x)^n\left(\mathbf{f}_i^n - \mathbf{f}_{i-1}^n\right) = (\Delta x)^{n+1}\mathbf{s}(\mathbf{u}^{n+1}) \ , \tag{5.12}$$

where $\mathbf{f}_i^n$ depends on the solution $\mathbf{u}^n$ and on the velocity of the grid $v_i'^n$, which is defined as follows:

$$v_i'^n = v_0^n\left(1 - \frac{i}{N}\right) \ , \qquad i = 0, ...N \ . \tag{5.13}$$

In this way, the convective flux at the material boundary, i.e. $\mathbf{f}_0$, is automatically zero and, at the same time, the intervals are moved in such a way that they all have the same length $(\Delta x)^n$. It is to remark that v_i' coincides with the material velocity of the solid only at the left boundary. The position of the i-th point at time $n+1$ is $x_i^n + v_i'^n\Delta t$ and the spatial integration step $(\Delta x)^{n+1}$ is

$$\begin{aligned}(\Delta x)^{n+1} &= (x_i^n + v_i'^n\Delta t) - (x_{i-1}^n + v_{i-1}'^n\Delta t) = \\ &= \left[x_i^n + v_0^n\left(1 - \frac{i}{N}\right)\Delta t\right] - \left[x_{i-1}^n + v_0^n\left(1 - \frac{i-1}{N}\right)\Delta t\right] = (\Delta x)^n - v_0^n\frac{\Delta t}{N} \ .\end{aligned} \tag{5.14}$$

In particular, if the integration intervals are initially equi-spaced, they remain equi-spaced at all the time steps.

The source term on the right hand side of equation (5.12) can be straightforwardly discretized implicitely, because it is not differential: when first computing ϕ^{n+1}, the implicit discretization of s^{n+1} can be easily performed, because s depends linearly on q, as may be seen in (5.9).

To impose proper boundary conditions, we observe that the mass and convective momentum flux on both sides of the sponge must be null; moreover, at the left boundary the sponge is in its relaxed state, while the stress at the right boundary is unknown. Therefore the flux vector on the boundary is imposed as follows:

$$\mathbf{f}_0^n = (0, 0), \qquad \mathbf{f}_N^n = (0, \Sigma(\phi_{N-1}^n)) \ . \tag{5.15}$$

The form of the discrete flux $\mathbf{f}_i^n$ that we have used in the interior of the domain is still to be defined. We do not go into details about this, just mentioning that a numerical approach which is well suited for non linear conservation laws has been adopted, namely, the numerical flux is computed by a second order upwind scheme, exploiting a characteristic decomposition of the jacobian of the function $\mathbf{f}(\mathbf{u})$ [27] (see also [28] for the basic mathematical background). This technique avoids unphysical oscillations in the solution, even if it has a discontinous behavior, as it happens in the present case when the liquid starts infiltrating.

The numerical method could be controlled by computing the total mass of the solid preform

$$M = \int_{x_f(t)}^{x_i(t)} \rho_s \phi_s^w(x,t)\, dx + \int_{x_i(t)}^{L} \rho_s \phi_s^d(x,t)\, dx\ .$$

However, summing up Eqs.(5.12) for $j = 1, \ldots, N$ it is immediately found that the mass is exactly conserved by the present approach.

In the simulations which follow we will use, as a starting point, stress-strain and permeability-volume ratio relations similar to the one measured by Sommer and Mortensen [10] for a polyurethane sponge (see Eq.(4.12) and Fig. 2). In order to examine the possible scenarios that might present, in the simulations we will, however, test the model considering several flow conditions characterized by different values of the dimensionless parameters. This corresponds to multiplying these quantities by suitable constants, still keeping the form of the constitutive relations.

Figure 5 presents a simulation obtained for given u_{in} corresponding to $\mathcal{P} = 4 \cdot 10^{-5}$ and $\mathcal{S} = 100$ in (a) and to $\mathcal{P} = 4 \cdot 10^{-4}$ and $\mathcal{S} = 50$ in (b). The figures on the left give the evolution of the volume ratio versus x at different times t_i. Those on the right give the position of the infiltration front $x_i(t)$ and of the boundary of the preform $x_f(t)$. In both cases the preform gradually compresses, and the position of the preform boundary monotonically increases. The infiltration front $x_i(t)$, which can be easily identified in the graphs on the left locating the discontinuity in the slope of the solution $\phi_s(x, t_i)$, travels at a nearly constant speed. It has to be remarked that the volume ratio in the dry region is nearly space independent, but depends on time. After $x_i(t)$ has reached the other end of the sponge, which, in dimensionless terms, occurs for $t = 1 - \phi_r$, in agreement with the theoretical predictions, the solution tends to the stationary configuration determined in Section 4. The behaviors in (a) and (b) are qualitatively similar but for the fact that, as expected, smaller $\mathcal{S}$ give rise to much stronger deformations.

In Fig. 6 the flow is driven by a constant pressure jump between the extrema of the solid preform. In the caption, a pedix P is added to $\mathcal{S}$ to avoid confusing this value with the one defined for given inflow velocities and also used in Section 4. The two values are linked, in the stationary case, by the integral relation (4.15), which relates the steady inflow velocity and the pressure drop.

As already stated at the end of Section 3, at the very beginning, the applied pressure difference generates a very high inflow velocity (say, up to $10\ m/s$), due to the smallness of air viscosity and of the infiltrated layer. Then, the elastic preform suddenly compresses. Due to the hyperbolic character of the evolution equation, which is in turn related to the elastic nature of the preform, a compression front, evident in Fig. 6b for $t = 0.005$, propagates into the sponge at a dimensionless speed of the order of $\sqrt{\mathcal{S}_P/\mathcal{P}}$. The speed, however, is not constant, since it depends on $\widetilde{\Sigma}'(\phi_s)$. Due to its elasticity, after compressing the preform expands back, generating oscillations in the location of the interfaces having period related to the time needed for the compression-rarefaction wave to travel back and forth between the borders of the preform (see the figures on the right). Referring to [14] and [20] for a more detailed discussion, it is possible to state that these effects will be strongly smoothed out if the solid preform were more properly modelled as a Voigt-Kelvin solid or as an anelastic solid. In this last case the system of equations would still be hyperbolic, but a stronger attenuation factor would be present. In the mean the preform compresses and then partially expands back. It has to be remarked that even when the oscillations die away, the infiltration velocity is not constant. The

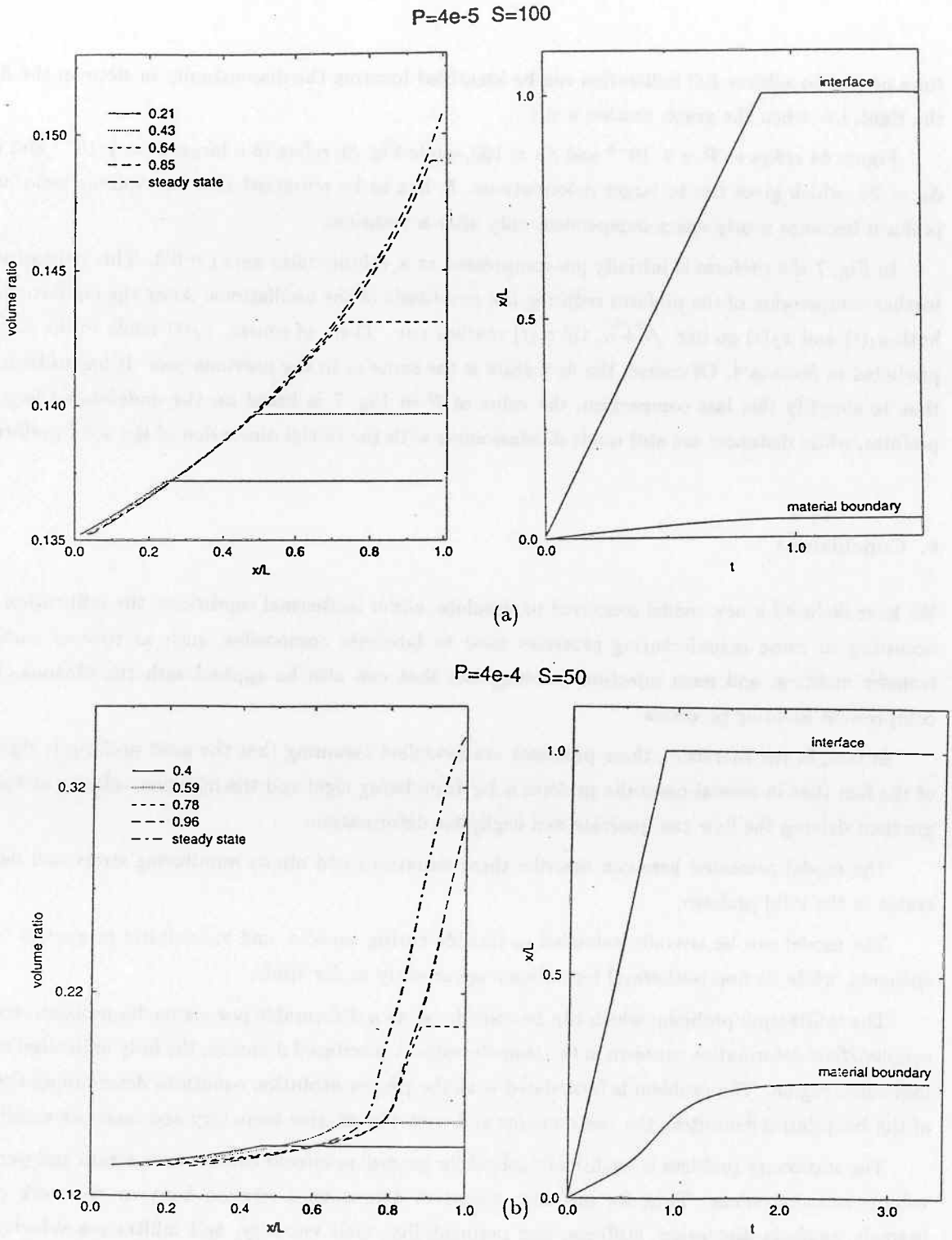

Figure 5 — Infiltration in an initially relaxed preform due to a constant inflow velocity corresponding to $\mathcal{P} = 4 \cdot 10^{-5}$ *and* $\mathcal{S} = 100$ *in (a) and to* $\mathcal{P} = 4 \cdot 10^{-4}$ *and* $\mathcal{S} = 50$ *in (b). On the left, the volume ratio is plotted at different times. The discontinuity in slope locates the advancing front* $x_i(t)$ *separating the wet and the dry region. On the right, the temporal evolution of the infiltration front* $x_i(t)$ *and of the material boundary* $x_f(t)$ *is given.*

time needed to achieve full infiltration can be identified locating the discontinuity in slope in the figures on the right, i.e. when the graph reaches $x = 1$.

Figure 6a refers to $\mathcal{P} = 4 \cdot 10^{-5}$ and $\mathcal{S}_P = 100$, while Fig. 6b refers to a larger $\mathcal{P} = 4 \cdot 10^{-4}$ and a smaller $\mathcal{S}_P = 25$, which gives rise to larger deformations. It has to be remarked that the volume ratio in the dry preform becomes nearly space independent only after a transient.

In Fig. 7 the preform is initially pre-compressed at a volume ratio $\phi_0(x) = 0.3$. This reduces the initial further compression of the preform reducing the amplitude of the oscillations. After the oscillations die out, both $x_i(t)$ and $x_f(t)$ go like $\sqrt{t + \alpha}$, till $x_i(t)$ reaches one. Then, of course, $x_f(t)$ tends to the steady value predicted in Section 4. Of course, the final state is the same as in the previous case. It has to be mentioned that to simplify this last comparison, the value of $\mathcal{P}$ in Fig. 7 is based on the undeformed length of the preform, while distances are still made dimensionless with the initial dimension of the solid preform.

6. Conclusions

We have deduced a new model conceived to simulate, under isothermal conditions, the infiltration problems occurring in some manufacturing processes used to fabricate composites, such as squeeze casting, resin transfer molding, and resin injection molding, but that can also be applied with the obvious changes to compression molding processes.

In fact, in the literature, these processes are modelled assuming that the solid preform is rigid, in spite of the fact that in several cases the preform is far from being rigid and the injection velocity or the pressure gradient driving the flow can generate non negligible deformation.

The model presented here can describe these situations and allows monitoring stress and deformation states in the solid preform.

The model can be trivially extended to include curing aspects, and viscoelastic properties of the constituents, while its non-isothermal formulation is currently under study.

The infiltration problem, which can be considered as a deformable porous media problem, consists in a coupled/flow deformation problem in two time-dependent interfaced domains, the fully infiltrated and the uninfiltrated region. The problem is formulated with the proper evolution equations determining the positions of the boundaries delimiting the two domains and with the relative boundary and interface conditions.

The stationary problem is analitically solved for general nonlinear elastic stress-strain and permeability-volume ratio relations. This, for instance, allows to determine a relation between the work parameters (namely, preform dimension, stiffness, and permeability, melt viscosity, and infiltration velocity) and the overall compression of the preform and its maximum deformation, of course in the steady state, which represents a starting point for a general description of the physical situations that will ultimately present.

Finally, the unsteady problem is solved by finite differences methods using upwind methods based on characteristic decomposition.

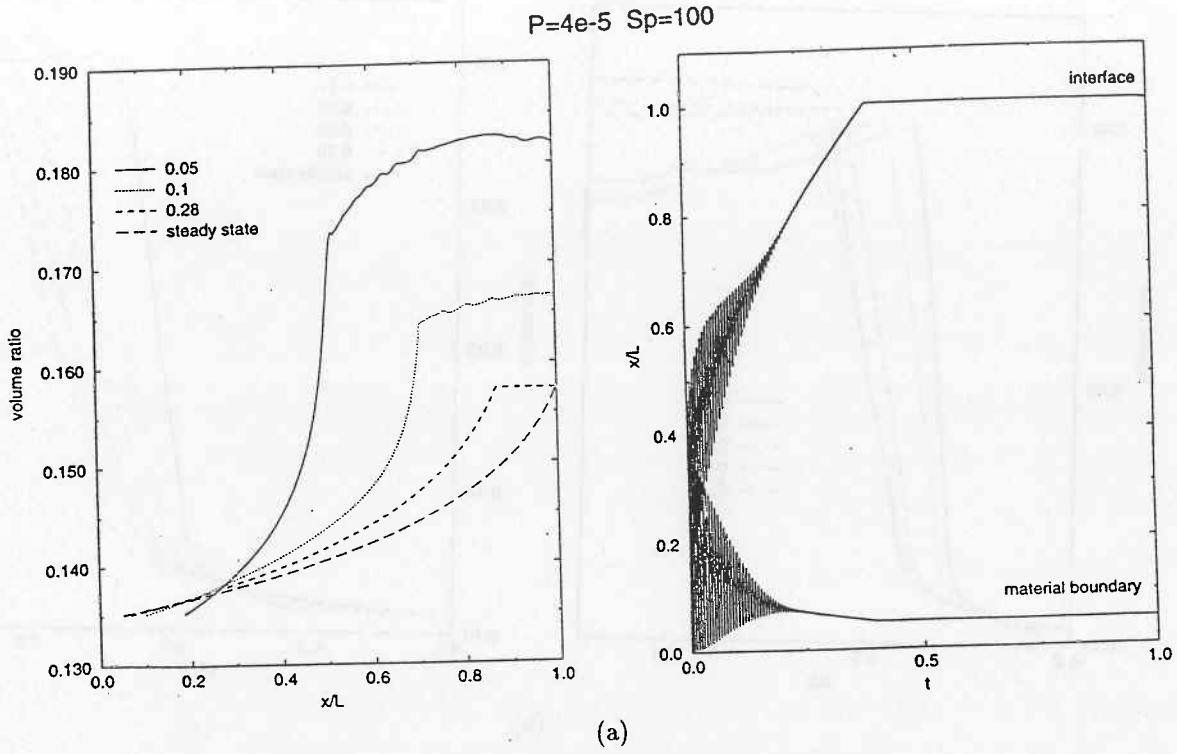

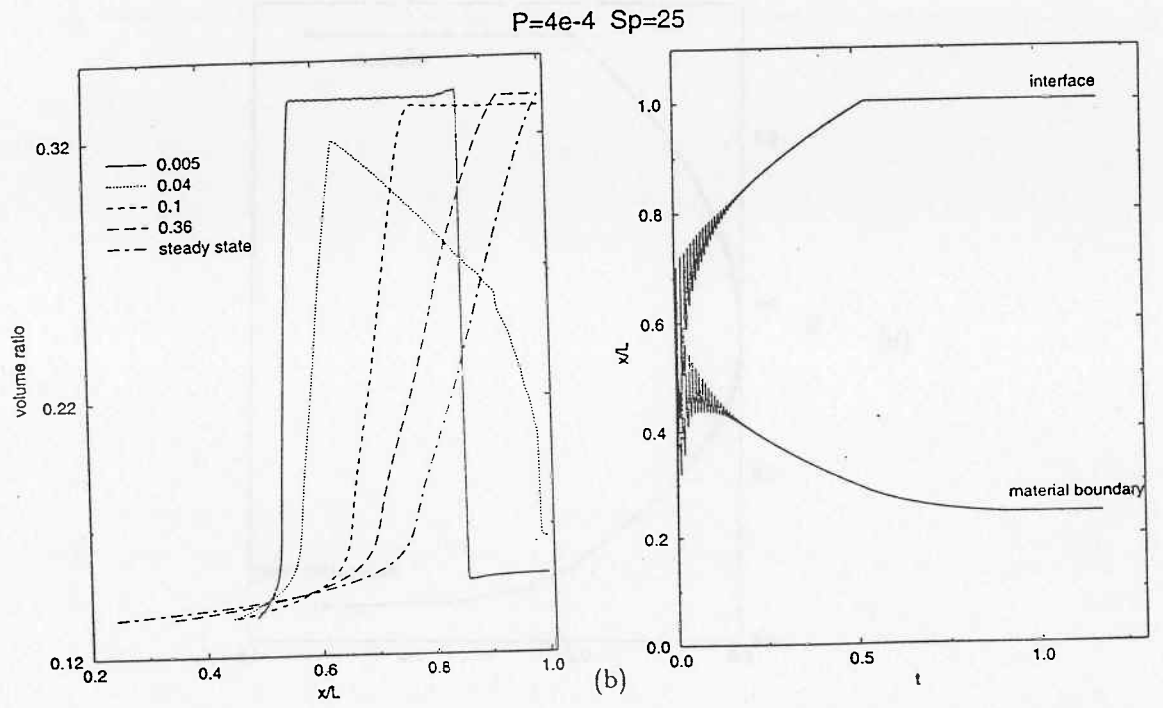

Figure 6 — Infiltration in an initially relaxed preform due to a constant pressure drop corresponding to $\mathcal{P} = 4 \cdot 10^{-4}$ *and* $\mathcal{S}_P = 25$ *in (a) and to* $\mathcal{P} = 4 \cdot 10^{-5}$ *and* $\mathcal{S}_P = 100$ *in (b). On the left, the volume ratio is plotted at different times. The initial sudden compression at the preform end generates a compression front propagating into the sponge, which is evidentiated in (b) for* $t = 0.005$. *The discontinuity in slope locates the advancing front* $x_i(t)$ *separating the wet and the dry region. On the right, the temporal evolution of the infiltration front* $x_i(t)$ *and of the material boundary* $x_f(t)$ *is given. The preform is fully infiltrated when* $x_i(t) = 1$. *The oscillations of the interfaces are due to the elasticity of the preform.*

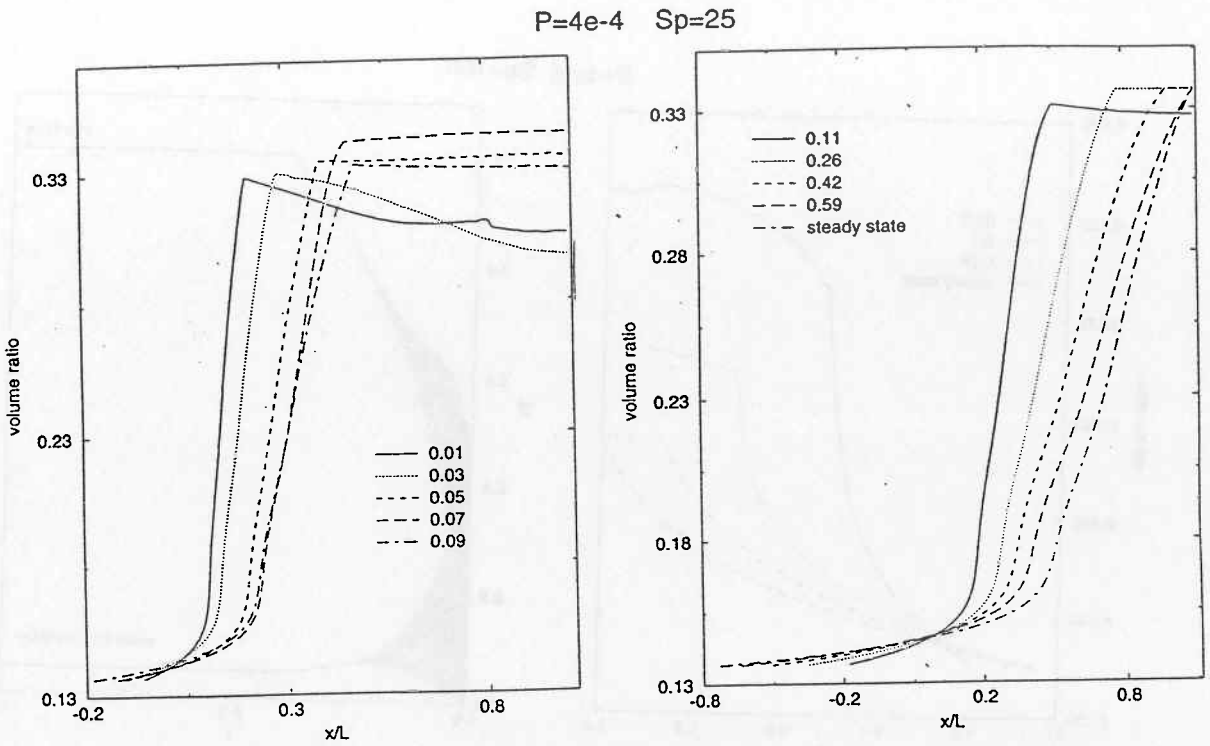

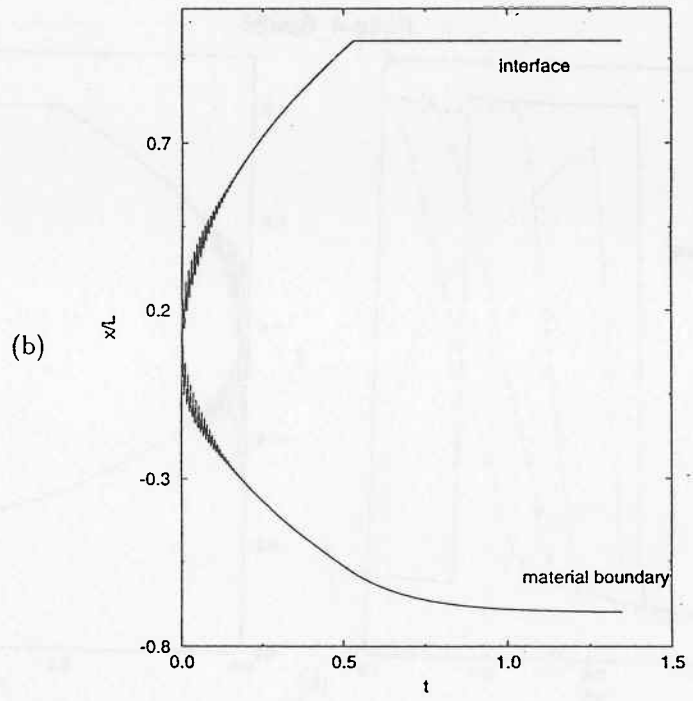

Figure 7 — Infiltration in a preform initially compressed at a volume ratio $\phi_0(x) = 0.3$ due to a constant pressure drop corresponding to $\mathcal{P} = 4 \cdot 10^{-4}$ and $\mathcal{S}_P = 25$. (a) Volume ratio at different times. The discontinuity in slope locates the advancing front $x_i(t)$ separating the wet and the dry region. The temporal evolution of $x_i(t)$ and of the material boundary $x_f(t)$ is given in (b). The preform is fully infiltrated when $x_i(t) = 1$. The initial sudden compression is not as strong a in Fig. 6, and therefore generates smaller oscillations.

Acknowledgements. The authors are grateful to the Italian National Research Council (C.N.R.), to the Italian Ministry for the University and Scientific Research (M.U.R.S.T.) and to the Sardinian Regional Authorities for funding the present research.

References

[1] Gonzalez-Romero, V.M., and Macosko, C.W., Process parameters estimation for structural reaction injection molding and resin transfer molding, *Polym. Engng. Sci.*, **30**, 142–146, (1990).

[2] Han, K., Lee, L.J., and Liou, M.J., Fiber mat deformation in liquid composite molding. II: Modeling, *Polymer Compos.*, **14**, 151–160, (1993).

[3] Han, K., Trevino, L., Lee, L.J., and Liou, M.J., Fiber mat deformation in liquid composite molding. I: Experimental analysis, *Polymer Compos.*, **14**, 144–150, (1993).

[4] Kim, Y.R., McCarthy, S.P., and Fanucci, J.P., Compressibility and relaxation of fiber reinforcements during composite processing, *Polymer Compos.*, **12**, 13–19, (1991).

[5] Lacoste, E., Aboulfatah, M., Danis, M., and Girot, F., Numerical simulation of the infiltration of fibrous preforms by a pure metal, *Metall. Trans.*, **24A**, 2667–2678, (1993).

[6] Lacoste, E., Danis, M., Girot, F., and Quennisset, J.M., Numerical simulation of the injection moulding of thin parts by liquid metal infiltration of fibrous preform, *Mater. Sci. Engng.*, **A135**, 45–49, (1991).

[7] Mortensen, A., and Wong, T., Infiltration of fibrous preforms by a pure metal: Part III. Capillary phenomena, *Metall. Trans.*, **21A**, 2257–2263, (1990).

[8] Rudd, C.D., and Kendall, K.N., Towards a manufacturing technology for high-volume production of composite components, *Proc. Instn. Mech. Engrs.*, **206**, 77–91, (1992).

[9] Rudd, C.D., Owen, M.J., and Middleton, V., Effects of process variables on cycle time during resin transfer moulding for high volume manufacture, *Mater. Sci. Techn.*, **6**, **656–665**, (1990).

[10] Sommer, J.L., and Mortensen, A., Forced unidirectional infiltration of deformable porous media, *J. Fluid Mech.*, **311** 193–215, (1996).

[11] Trevino, L., Rupel, K., Young, W.B., Liou, M.J., and Lee, L.J., Analysis of resin injection molding in molds with preplaced fiber mats. I: Permeability and compressibility measurements, *Polymer Compos.*, **12**, 20–29, (1991).

[12] Yamauchi, T., and Nishida, Y., Infiltration kinetics of fibrous preforms by aluminum with solidification, *Acta Metall. Mater.*, **43**, 1313–1321, (1995).

[13] Young, W.B., Rupel, K., Han, K., Lee, L.J., and Liou, M.J., Analysis of resin injection molding in molds with preplaced fiber mats. II: Numerical simulation and experiments of mold filling, *Polymer Compos.*, **12**, 30–38, (1991).

[14] Preziosi, L., The theory of deformable porous media and its application to composite material manufacturing, *Surveys in Mathematics for Industry*, (1996). To appear.

[15] Parker, K.H., Mehta, R.V., and Caro, C.G., Steady flow in porous, elastically deformable materials, *J.*

Appl. Mech., **54**, 794–800, (1987).

[17] Clyne, T.W., and Mason, J.F., The squeeze infiltration process for fabrication of metal-matrix composites, *Metall. Trans.*, **18A**, 1519–1530, (1987).

[16] Reboredo, M.M., and Rojas, A.J., Molding by reactive injection of reinforced plastics, *Polymer Engng. Sci.*, **28**, 485–490, (1988).

[18] Rajagopal, K.R., and Tao, L., **Mechanics of Mixtures**, World Scientific, (1995).

[19] Bowen, R.M., Incompressible porous media models by use of the theory of mixtures, *Int. J. Engng. Sci.*, **18**, 1129–1148, (1980).

[20] Preziosi, L., Joseph, D.D., and Beavers, G.S., Infiltration in initially dry, deformable porous media, *Int. J. Multiphase Flows*, (1996), in press.

[21] Beavers, G.S., Hajii, A., and Sparrow, E.M., Fluid flow through a class of highly-deformable porous media: Part I – Experiments with air, *J. of Fluids Eng.*, **103**, 432–439, (1981).

[22] Beavers, G.S., Wilson, T.A., and Masha, B.A., Flow through a deformable porous material, *J. Appl. Mech.*, **42**, 598–602, (1975).

[23] Beavers, G.S., Wittenberg, K., and Sparrow, E.M., Fluid flow through a class of highly-deformable porous media: Part II – Experiments with water, *J. of Fluids Eng.*, **103**, 440–444, (1981).

[24] Liu, I.S., On chemical potential and incompressible porous media, *J. Mécanique*, **19**, 327–342, (1980).

[25] Müller, I., Thermodynamics of mixtures of fluids, *J. Mécanique*, **14**, 267–303, (1975).

[26] Vinokur, M., An analysis of finite-difference and finite-volume formulations of conservation laws, *J. Comp. Phys.*, **81**, 1–52, (1989).

[27] LeVeque, R.J., **Numerical Methods for Conservation Laws**, Birkhäuser Verlag, Zurich, (1992).

[28] Bellomo, N., and Preziosi, L., **Modelling, Mathematical Methods and Scientific Computation**, CRC Press, Boca Raton, (1995).